Influence of relative humidity and loading frequency on the PA6.6 thermomechanical cyclic behavior: Part II. Energy aspects

Adil Benaarbia, André Chrysochoos, Gilles Robert

Influence of relative humidity and loading frequency on the PA6.6 thermomechanical cyclic behavior: Part II. Energy aspects

Adil Benaarbia [a, b, *], André Chrysochoos [a], Gilles Robert [b]

[a] University Montpellier 2, LMGC laboratory, CNRS, Place Eugène Bataillon, 34095 Montpellier, France
[b] Solvay Engineering Plastics, Technyl Innovation Center-Simulation et Validation des Applications, Avenue Ramboz – BP64, 69192 Saint Fons, France

A B S T R A C T

In this study, we investigated the influence of relative humidity (RH) and loading rate on the energy response of PA6.6 matrix specimens. The latter were subjected to oligocyclic tensile-tensile tests at 3 different RH and 2 loading rates. Infrared thermography was used to obtain a direct estimate of heat sources using the heat diffusion equation. Using the mechanical and thermal responses discussed in the first part of this work, complete energy rate balances were drawn up. In particular, the time courses of deformation, and dissipated and stored energy rates are discussed. The strong influence of the loading frequency and RH on the energy storage mechanisms is also highlighted.

Keywords:
PA6.6 matrix
Relative humidity
Dissipated and stored energy
Quantitative infrared calorimetry

1. Introduction

Energy analysis regarding deformation mechanisms is of particular interest in the mechanics of materials. It provides useful guidelines for improving constitutive material models. A constitutive model correctly describing deformation mechanisms should also properly predict the amounts of stored and dissipated energy, as well as the ranges of the thermomechanical coupling heat sources. Stored energy stands for the internal energy variations associated with the material microstructural changes, while dissipated energy highlights the nature and intensity of irreversibility accompanying deformation. Coupling heat sources overlap with dissipation and reflect possible interactions between the microstructural and hygro-thermo-mechanical states of the material.

Some interesting (historical) surveys on specific aspects of the energy behavior can be found in the literature [1]). The most significant developments that have taken place in the assessment and interpretation of stored vs. dissipated energy and coupling heat sources have relied closely on calorimetric procedures. From an experimental standpoint, as the stored energy is not directly accessible, an indirect way to estimate these internal energy variations using thermal data is often proposed. Most research has been focused on temperature rise measurements to estimate variations in stored and/or dissipated energy using different experimental equipment, ranging from embedded thermocouples, microcalorimeters to infrared detectors [2–10]. With IR thermal data, the heat diffusion equation is now widely used to estimate dissipated heat locally involved during deformation process [11,12–15].

For standard (homogeneous) mechanical tests, deformation energy assessments can be conventionally carried out using stress and strain signals. Both heat and deformation energy assessments can then be combined to estimate the stored energy, thus establishing complete energy

* Corresponding author. University Montpellier 2, LMGC laboratory, CNRS, Place Eugène Bataillon, 34095 Montpellier, France.
E-mail addresses: abenaarb@univ-montp2.fr, adil.benaarbia@etud.univ-montp2.fr (A. Benaarbia).

balances. More recently, for uniaxial tests on thin flat specimens, full field kinematic measurements by digital image correlation were used to estimate distributions of strain and stress within a sample gage part, with the stress fields being derived from kinematic data via momentum equations [16]. From a calorimetric standpoint, the development of infrared measurement techniques has also enabled reliable measurement of temperature fields on the specimen surface. The use of temperature fields provides an opportunity to observe thermal signatures of multiple and combined physical phenomena occurring during deformation processes [17]. However, temperature variations are not totally intrinsic to the material behavior, i.e. they depend on the heat source intensity and distribution, as well as the diffusion properties and thermal boundary conditions. Heat sources can be derived from thermal data by estimating differential operators of the heat diffusion equation [18,19]. As the only thermal information provided by an IR camera is in-plane temperature fields, several regularizations and assumptions about the heat source distribution have been formulated to make heat diffusion models operational. Many simplified formulations are now available to deal with heat source assessments. Hypotheses put forward to assess heat sources were recently summarized in [15] for the PA6.6 energy behavior analysis.

Indeed, this study is right in line with previous studies on dry and humid PA6.6 specimens [20]. The studies dealt with the influence of relative humidity and loading frequency on the mechanical and thermal responses. The goal is now to achieve energy balances under different hygromechanical loading conditions. After a brief description of the thermomechanical background and experimental protocol, we discuss the energy behavior of PA6.6 specimens under different mechanical loadings. We thus documented and analyzed the complete energy balances associated with different fatigue tests, as well as the contribution of the mean stored energy rate per cycle. The paper ends with a discussion on many different findings noted during this exploratory work.

2. Thermodynamic aspects

The deformation energy $\mathscr{W}_{def}$ developed during material deformation can be split into the elastic $\mathscr{W}_e$ and anelastic energies $\mathscr{W}_{an}$, where $\mathscr{W}_{an}$ is both stored $\mathscr{W}_s$ and dissipated $\mathscr{W}_d$. This deformation energy reads:

$$\mathscr{W}_{def} = \mathscr{W}_e + \mathscr{W}_s + \mathscr{W}_d \tag{1}$$

The quantification of these energies (e.g. deformation, dissipated and stored) involved during thermomechanical deformation of polymeric materials is of substantial interest to gain further insight into fatigue mechanisms. Determining the proportions of dissipated and stored deformation energy is, as already mentioned, of particular interest. Dissipated energy reflects the irreversibility that accompanies the fatigue process, whereas the stored energy quantifies internal energy variations induced by microstructural transformations. Note that this stored energy may be released during possible unloading or restoration processes.

The heat diffusion equation is essential for estimating heat source fields. To estimate these heat sources and carry up quantitative analysis, the thermodynamics of irreversible processes (TIP) framework was adopted [21]. In this thermodynamic context, the complete local expression of the heat diffusion equation can be directly obtained as follows:

$$\rho C_{\boldsymbol{\varepsilon},\boldsymbol{\alpha}}\dot{T} + \operatorname{div}\left(\underbrace{-\boldsymbol{k}\, grad T}_{q}\right) = \underbrace{\left(\boldsymbol{\sigma} - \rho\boldsymbol{\psi}_{,\boldsymbol{\varepsilon}}\right) : \dot{\boldsymbol{\varepsilon}} - \rho\psi_{,\alpha_k}\dot{\alpha}_k}_{\mathscr{D}_1} + \underbrace{\rho T\boldsymbol{\psi}_{,T,\boldsymbol{\varepsilon}} : \dot{\boldsymbol{\varepsilon}} + \rho T\psi_{,T,\alpha_k}\dot{\alpha}_k}_{\mathscr{W}'_c} + r_e \tag{2}$$

where T and ε are, respectively, the absolute temperature and strain tensor, whereas α_k ($k = 1,\ldots,N$) represents the N internal state variables, pooled in vector α and introduced to describe the microstructural state. The material constants ρ, k and $C_{\boldsymbol{\varepsilon},\boldsymbol{\alpha}}$ are the material density, the heat conduction tensor and the specific heat at constant ε and α_k. The state function ψ represents the specific Helmholtz free energy and r_e is the heat supply term characterizing a volume heat exchange with the surroundings. The $\mathscr{D}_1$ term stands for the mechanical intrinsic dissipation and $\mathscr{W}'_c$ for the possible thermomechanical coupling sources. Note that the nonstandard notation $(.)'$ specifies that $(.)$ is path-dependent. When $\mathscr{W}'_c$ represents the thermomechanical coupling source, then this energy is not a state function.

Since the experimental data provided by infrared cameras are 2D temperature maps, it could be relevant to reduce the above 3D expression of the heat diffusion equation to at least a 2D diffusion problem before assessing the different heat sources. To do so, a set of assumptions was taken into account in order to draw up simplified heat diffusion models describing heat transfers between loaded specimens and the surroundings [18]. The simplification was based on an average of the 3D heat diffusion equation over one (thickness) or two (thickness and width) directions. In the important case of quasi-homogenous tests, if a uniform distribution of heat sources can sometimes be reasonably assumed, a 0D formulation of the heat diffusion equation could be proposed [18]. The diffusion equation then becomes a simple differential equation corresponding to the first eigen function of the spectral solution of the 3D heat diffusion model. Naturally, the choice of such simplified models highly depends on the type of experimental investigation. The 2D diffusion model is preferable for highly heterogeneous situations. The 1D diffusion model may be sufficient when heat sources are uniformly distributed over each cross-section of the specimen. In the following, we chose the 0D formulation that is less sensitive to thermal noise and less time consuming in terms of heat source computation. As already underlined, this approach is well adapted to (quasi) homogeneous tests when rapid experimental estimates of heat sources are required. The simplified 0D model is given by the following expression:

$$\rho C_{\boldsymbol{\varepsilon},\boldsymbol{\alpha}}\left(\langle\dot{\theta}\rangle + \frac{\langle\theta\rangle}{\tau_{\text{th}}^{0d}}\right) = \langle\mathscr{D}_1\rangle + \langle\mathscr{W}'_c\rangle \tag{3}$$

where $\theta = T - T_o$ is the temperature variation averaged over the volume element under investigation (with T_o denoting the initial temperature field), τ_{th}^{0d} is a time constant characterizing overall heat exchanges between this volume element and the surroundings. On the right hand side of Eq. 3, we find the mean intrinsic mechanical dissipation $\mathscr{D}_1$ and thermomechanical coupling sources $\mathscr{W}'_c$ averaged over the same volume element.

3. Experimental set-up and procedures

3.1. Material and loadings

The polymer investigated in this study was the polyamide 6.6 matrix manufactured by Solvay Engineering Polyamides. Test samples were 100 × 20 mm in length and width and 3.14 mm in thickness (see Fig. 1 (a)). Three relative moisture levels were considered: RH0 (dry-as-molded specimens), RH50 (i.e. 50% relative humidity), and RH80. All specimens were sealed prior to testing to maintain and provide a controlled uniform humidity.

Cyclic uniaxial tensile-tensile tests were carried out using a MTS 810 hydraulic testing machine equipped with a ± 25 kN load cell. All experiments were conducted at room temperature (23 °C). The cyclic tensile-tensile loads were carried out under a stress ratio R_σ of 0.1, where $R_\sigma = \sigma_{min}/\sigma_{max}$. The loading frequencies were l 1 Hz and 10 Hz, while the number of cycles was set at 10^4. The studied cyclic mechanical loading is illustrated in Fig. 1 (b).

3.2. Temperature field measurement procedure

Infrared thermography is a convenient non-contact imaging technique that uses an infrared sensor to visualize and estimate temperature fields on material surfaces. The principle of the technique is based on use of the intensity and wavelength of radiation emitted by the loaded material to measure its surface temperature according to Planck's law.

The infrared thermal imaging system used for thermographic measurement was a CEDIP Jade camera cooled by a Stirling cooler. This contained an InSb detector which is sensitive to infrared radiation in the 3–5μm wavelength range. The camera was equipped with a 25mm lens and positioned on a tripod approximately 0.5 m from the specimen surface. We decided to operate the detector with a 160 × 128 pixel window size, 29μm pixel size and 1800μs integration time. The frame rate of camera was set at ten times the loading frequency to obtain enough sampled data to improve the signal-to-noise ratio using local least-squares approximation. Thus, the loading frequency was set at 1Hz (resp. 10 Hz) and the frame rate was set at 10 frames (resp. 100 frames) per second.

During the experiments, several factors complicated measurement of the surface temperature of the investigated materials. Several experimental precautions were thus taken to overcome these difficulties. Readers interested in these tricky metrological aspects are referred to the first part of this work [20].

Even although these precautions were taken, the measured data were not necessarily quantitative and the true temperature value could not be derived directly. An appropriate calibration protocol was thus conducted to determine the reliable temperature values. This allowed conversion of the thermal radiation digitized by the infrared camera into temperature using pixel calibration functions [22]. This pixel protocol was based on a polynomial fitting of the digital levels $\mathscr{DL}_{(m,n)}$, delivered by each individual detector element (m,n) using a black body with a uniform high emissivity coating, maintained at cold and hot temperatures $T_{(m,n)}$. The measurement accuracy could thus be assessed for each pixel individually in the resulting image.

$$T_{(m,n)} = \sum_{k=0}^{d_f} \varkappa_{(m,n)_k} \mathscr{D}\mathscr{L}^k_{(m,n)} \tag{4}$$

where d_f denotes the degree of the polynomial fitting function and $\varkappa_{(m,n)k}$ are coefficients of the calibration law for the element (m,n). These coefficients were derived from least squares fitting approximations.

Two bad pixel detection criteria were used. The first consisted of the elimination of pixels whose response predicted by the polynomial fitting $T_{(m,n)}$ was far from the ordered temperature of the used black body T_{bb}, whereas the thermal response of the second eliminated pixels was too far from the calculated average temperature throughout the detector T_{av}. In agreement with the foregoing, both criteria were written as:

$$\left|T_{(m,n)} - T_{bb}\right| \geq \delta T_1, \quad \left|T_{(m,n)} - T_{av}\right| \geq \delta T_2 \tag{5}$$

where δT_1 and δT_2 were respectively the threshold values of the first and second criteria.

The room temperature was taken into account by recording the temperature data of an unloaded specimen

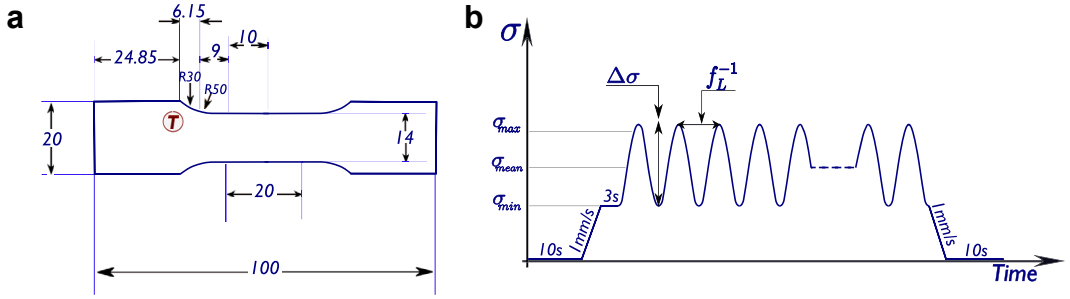

Fig. 1. (a) Shape of the specimens used for the experiments (all dimensions are in millimeters). (b) Diagram of the mechanical loading used in the experiments.

(*dummy*) kept nearby the test specimen. The temperature images were then acquired using *Altair* software and stored on a computer hard drive. A local least-square fitting method using an optimized approximation function set was developed to filter the IR images from the noise [18].

4. Experimental results

4.1. Energy balances during oligocyclic fatigue tests

The energy responses of the cyclic thermomechanical behavior of the PA6.6 matrix are shown and discussed in this section. We focused only on the 3 selected hygro-thermal states (relative humidity: RH0, RH50 and RH80), 2 loading rates ($f_L = 1$ and 10 Hz) and 2 stress levels (high and low levels with $R_\sigma = 0.1$). In each case, the energy balance was drawn up and the corresponding mean values of the stored energy ratio (i.e. the Taylor-Quinney coefficient) were computed.

The deformation energy rate averaged over the specimen gage part and over a complete cycle $\tilde{\mathscr{W}}'_{def}$ was computed, as well as the mean stored energy rate $\tilde{\mathscr{W}}'_{s}$ and the mean dissipation $\tilde{\mathscr{D}}_1$. The mean elastic energy rate over a cycle $\tilde{\mathscr{W}}'_{e}$ was neglected. All energies were computed using selected experimental data. The mechanical energy rate per cycle $\tilde{\mathscr{W}}'_{def}$ was estimated using the following expression:

$$\tilde{\mathscr{W}}'_{def} = \frac{f_L \kappa}{\mathscr{V}_g} \oint_{cycle} F\, dl \tag{6}$$

where F and l are, respectively, the applied force (given by the load cell signal) and the current length of the specimen gage part (given by an optical extensometer), and $\mathscr{V}_g$ is the volume of the gage area. κ represents a geometrical ratio characteristic of the specimen. This ratio connects the global mechanical response to the local one based on the hypothesis that the deformation process gives a homogeneous stress state over each cross-section. This was defined and computed using the following definition:

$$\kappa = \int_{-\frac{L_0}{2}}^{\frac{L_0}{2}} l^{-1}(y)\, dy \Big/ \int_{-\frac{L}{2}}^{\frac{L}{2}} l^{-1}(y)\, dy \tag{7}$$

where L_o denotes the length of the gauge section, L represents the length of the deformed sample and $l(y)$ stands for the width of the specimen at the longitudinal coordinate y.

The mean dissipation heat source $\tilde{\mathscr{D}}_1$ values were derived from the integrated form of the heat equation over the considered gage part (see. Eq. 3). This mean dissipation, averaged over one complete cycle and divided by ρC, was computed using the following expression:

$$\frac{\tilde{\mathscr{D}}_1}{\rho C} = f_L \int_{(q-1)f_L^{-1}}^{qf_L^{-1}} \frac{\langle \mathscr{D}_1 \rangle}{\rho C} d\tau \tag{8}$$

where q stands for the cycle number.

This dissipative term was determined by estimating the derivative operator in Eq. 3 using IR thermal data. The noise component was eliminated from the data system record using local polynomial fitting functions based on least square techniques [11]. These fitting methods were essential to compute reliable estimates of dissipative heat sources but they are time-consuming and tricky to use [23].

The energy balance was first achieved for the 10 Hz loading frequency. All thermomechanical data were converted and used to compute and plot the energies in Fig. 2 (a-b-c). The dark curve corresponds to the mean deformation energy rate per cycle, the green curve represents the stored energy rate per cycle and the red curve indicates the mean intrinsic dissipation per cycle. All energies were plotted as a function of the cycle number. Note that the heat sources were divided by ρC, and thus expressed in $^\circ C.s^{-1}$. This operation enabled us to define, for each energy, an equivalent heating rate to facilitate the comparison between dissipative and stored energy rates.

- For a dry-as-molded matrix (RH0), a substantial part of the mean stored energy rate per cycle is shown in Fig. 2 (a). The corresponding Taylor-Quinney ratio at the end of the test has a mean value of about 75%. For RH50 and RH80, the results indicated in Fig. 2 (b-c) show that the energy storage decreased at the beginning of the cyclic loading and stabilized gradually at about 50% after around 2500 cycles. The comparison between energy balances for dry-as-molded and conditioned specimens indicated that, for a certain relative humidity threshold, the energy responses were no longer modified by the change in water content, as shown for both conditioned specimen experiments (RH50 and RH80). For RH50 specimens, the mean intrinsic dissipation increased at the beginning of loading and then stabilized after the first few cycles, with a ratio close to 50% (see. Fig. 2 (b)). This ratio had approximately the same values for specimens conditioned at RH80 (see. Fig. 2 (c)). These results confirmed and further emphasized the storage character of PA6.6 dry matrices at high loading rates [10]. However, for RH50 and RH80 specimens, the mean deformation energy rate per cycle was evenly stored and dissipated.
- In the case of low loading frequencies ($f_L = 1$ Hz), the dissipated and stored ratio trend changed completely, as it is outlined in Fig. 2 (d-e-f). In every case, the mean intrinsic dissipation per cycle became predominant compared with the stored energy rate. It started increasing suddenly at the beginning of loading and then stabilized after the first few hundreds of cycles, with a ratio of 90% for RH50 (see. Fig. 2 (e)) and 82% for RH80 (see. Fig. 2 (f)). Conversely, the total stored energy rate per cycle decreased during the first 500 cycles and then started to stabilize at around a ratio of 10% and 18%, respectively, for both conditioned specimens. These findings are in agreement with those obtained in [10], where the intrinsic dissipated energy rate per cycle was significantly greater (73%) than the stored energy rate per cycle for dry PA6.6 specimens subjected to a 1 Hz loading frequency.

4.2. Influence of the stress range on the energy rate balance form

So far, all aspects of the material energy response have been discussed while taking the loading frequency and

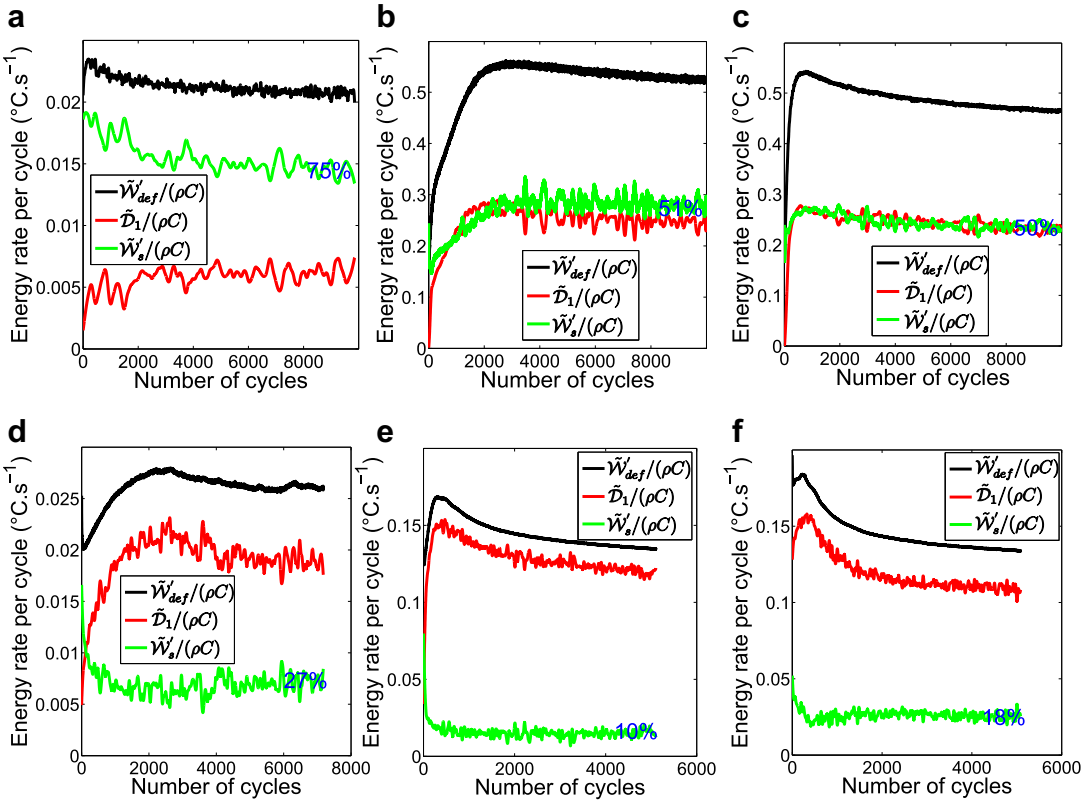

Fig. 2. Energy rate balances associated with cyclic tests performed on the PA6.6 matrix (a) RH0/10Hz, (b) RH50/10Hz, (c) RH80/10Hz, (d) RH0/1Hz, (e) RH50/1Hz and (f) RH80/1Hz, showing the effects of relative humidity and loading rate. The load ratio was $R_\sigma = 0.1$. The geometrical ratio was $\curlyvee = 0.437$ and the volume of the observed gauge area was $V_g = 753$ mm^3.

water content into account. More attention could also be paid to the kinetics of the energy behavior of the PA6.6 matrix as a function of the stress range. It is essential to be able to apply PA6.6 to industrial applications under complex stress conditions and this issue has to be addressed. Hereafter, two stress ranges ("high" and "low" stress ranges) are considered for the same stress ratio $R_\sigma = 0.1$. The results in Fig. 3 show time courses of the energy rate balance associated with dry polyamide 6.6 subjected to both cyclic stress loadings: a high stress range (Fig. 3 (a)) and a low stress range (Fig. 3 (b)), for a 10 Hz loading frequency.

- These results indicate that the storage character of the PA6.6 matrix varied slightly with the stress level. For low stress levels, the stored ratio stabilized at around 75%, contrary to the high stress levels whose stored ratio saved approximately 86%. In both instances, the stored energy rate per cycle prevailed over the mean intrinsic dissipation per cycle. It decreased at the beginning of loading, with an increase in the number of cycles, and then stabilized after enough cycles, i.e. 4000 cycles. It can be concluded that the energy storage remained high even for low stress levels with dry PA6.6 matrix specimens. This storage may correspond to microstructural changes (e.g. internal energy variation) and could lead to slow but regular material degradation.

4.3. Comparative analysis of the energy rate terms

A comparative presentation of energy rate values in dry-as-molded and conditioned specimens is given hereafter. The data presented in Fig. 4 show the mean intrinsic dissipation values per cycle (Fig. 4 (a)), the stored energy rate per cycle (Fig. 4 (b)) and the hysteresis loop area (Fig. 4 (c)), respectively.

It can be inferred that the increase in relative humidity led to an increase in the dissipation, and the stored and deformation energy rates per cycle. The mean stored energy rates and mean intrinsic dissipations were markedly higher for humid specimens compared with those of dry-as-molded specimens. Indeed, the stored energy rates for humid specimens were twentyfold higher than those of dry-as-molded specimens. The same trend was noted for the mean intrinsic dissipation and the mean deformation energy rate per cycle. Both of these energy rates had values of around 0.25 °C.s^{-1}, 0.5 °C.s^{-1} for RH80, and 0.27 °C.s^{-1}, 0.55 °C.s^{-1} for RH50, respectively. However, for dry-as-molded specimens, the values were 0.015 °C.s^{-1} and 0.023 °C.s^{-1}.

5. Concluding comments

In this paper, we analyzed the influence of the relative humidity, loading rate and stress level on the energy

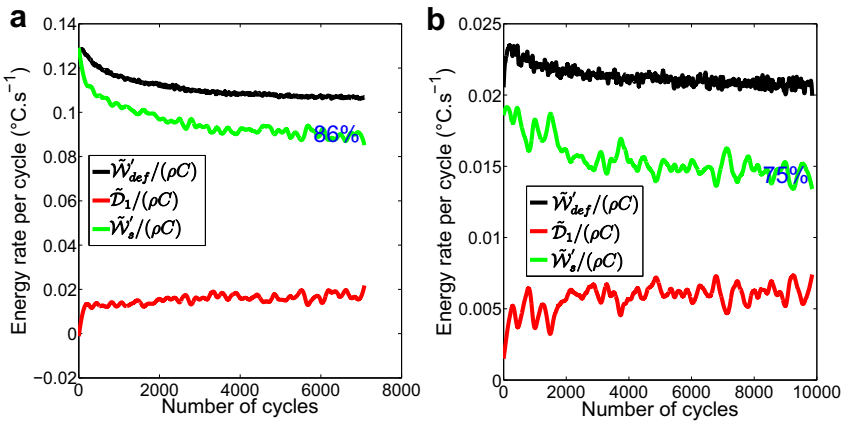

Fig. 3. The energy rate balances associated with cyclic tests performed on the dry PA6.6 matrix for two different stress ranges (a) RH0/10Hz/High stress range, (b) RH50/10Hz/Low stress range. The load ratio was $R_\sigma = 0.1$. The geometrical ratio was $\nu = 0.437$ and the volume of the observed gauge area was $V_g = 753$ mm^3.

behavior of semi-crystalline PA6.6 matrix. It was found that the relative humidity conditions and the loading frequency completely affected the form and kinetics of the energy rate balance. Regarding the humidity effects, although roughly 50% of stored energy was obtained for both preconditioned RH50 and RH80 specimens at high loading rates, the dry-as-molded specimen indicated a mean stored energy rate per cycle of approximately 70% of the deformation energy. The comparison between energy balances for dry as-molded and humid specimens suggested that for a certain relative humidity level, the energy responses were only slightly modified by the change in water content. Also, the loading frequency seemed to have a marked influence on the energy rate balance kinetics. Investigations on energy stored during deformation indicated that the stored ratio was significantly lower at low loading rates but remained high at high loading rates. These considerations are important regarding the inclusion of energy balance kinetics in constitutive PA6.6 matrix models. The insight that the stored energy can provide concerning structural changes due to the deformation mechanisms has to be enhanced. The next crucial question that needs to be addressed is: *does the stored energy have a permanent character? In other words, is it released or partly released after unloading? If so, what does this phenomenon so far imply in terms of modeling elements?*

Regarding the industrial applications of this work, further experiments are currently under way to gain further insight into these energy effects, especially in fiber-reinforced polymeric materials in which the fiber orientation effect has to be explored. These future investigations should also assess the role of humidity on the cyclic behavior of these composite materials compared with the role of temperature, as both effects (humidity and temperature) prompt an increase in the molecular mobility of the PA6.6 matrix.

Acknowledgements

The authors gratefully acknowledge Solvay Engineering Plastics for supporting this work and for providing material data and specimens. This work benefited from the financial

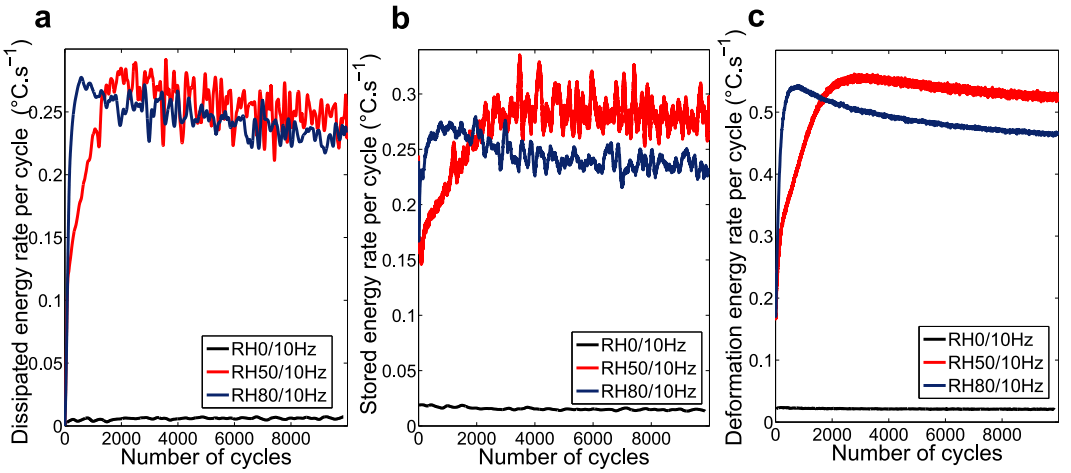

Fig. 4. Time courses of (a) the mean intrinsic dissipation per cycle, (b) the stored energy rate per cycle and (c) the mean mechanical energy rate per cycle for RH0, RH50 and RH80 conditioned specimens subjected to a 10 Hz loading frequency and a $R_\sigma = 0.1$ load ratio.

support of the French Minister for Research (ANRT) (CNRS079212:UM2 121532) and was performed in the framework of the European DURAFIP (F1201028V) project (FUI project supported by Oseo).

The authors also wish to warmly thank a very present but discrete partner, David Manley, for the many effective tips that significantly improved the presentation of our work.

References

[1] M. Bever, D. Holt, A. Titchener, The stored energy of cold work, Progress in Materials Science, 17, 1973. Pergamon, New York.
[2] G.I. Taylor, H. Quinney, The latent energy remaining in a metal after cold working, Proceedings of The Royal Society A: Mathematical Physical and Engineering Sciences 143 (1934) 307–326.
[3] A. Chrysochoos, Energy balance for elastic plastic deformation at finite strain (in French), Journal de Mécanique théorique et appliquée 5 (1985) 589–614.
[4] A. Chrysochoos, O. Maisonneuve, G. Martin, H. Caumon, J.C. Chezeaux, Plastic and dissipated work and stored energy, Nuclear Engineering and Design 114 (1989) 323–333.
[5] J. Mason, A. Rosakis, G. Ravichandran, On the strain and strain rate dependence of the fraction of plastic work converted to heat : an experimental study using high speed infrared detectors and the Kolsky bar, Mechanics of Materials 17 (1994) 135–145.
[6] R. Kapoor, S. Nemat-Nasser, Determination of temperature rise during high strain rate deformation, Mechanics of Materials 27 (1998) 1–12.
[7] D. Rittel, On the conversion of plastic work to heat during high strain rate deformation of glassy polymers, Mechanics of Materials 31 (1999) 131–139.
[8] P. Rosakis, A.J. Rosakis, G. Ravichandran, J. Hodowany, A thermodynamic internal variable model for the partition of plastic work into heat and stored energy in metals, Journal of The Mechanics and Physics of Solids 48 (2000) 581–607.
[9] W. Oliferuk, M. Maj, B. Raniecki, Experimental analysis of energy storage rate components during tensile deformation of polycrystals, Materials Science and Engineering A-structural Materials Properties Microstructure and Processing 374 (2004) 77–81.
[10] A. Benaarbia, A. Chrysochoos, G. Robert, Kinetics of stored and dissipated energies associated with cyclic loadings of dry polyamide 6.6 specimens, Polymer Testing 34 (2014) 155–167.
[11] B. Berthel, A. Chrysochoos, W. Wattrisse, A. Galtier, Infrared image processing for the calorimetric analysis of fatigue phenomena, Experimental Mechanics 48 (2008) 79–90.
[12] C. Doudard, S. Calloch, F. Hild, S. Roux, Identification of heat source fields from infra-red thermography: determination of 'self-heating' in a dual-phase steel by using a dog bone sample, Mechanics of Materials 42 (2010) 55–62.
[13] E. Charkaluk, A. Constantinescu, Dissipative aspects in high cycle fatigue, Mechanics of Materials 41 (2009) 483–494.
[14] J.R. Samaca Martinez, J.B. Le Cam, X. Balandraud, E. Toussaint, J. Caillard, Mechanisms of deformation in crystallizable natural rubber. Part 2: quantitative calorimetric analysis, Polymer 54 (2013) 2727–2736.
[15] A. Benaarbia, A. Chrysochoos, G. Robert, Fiber orientation effects on heat source distribution in reinforced polyamide 6.6 subjected to low cycle fatigue, Journal of Engineering Mathematics (2014). In press.
[16] B. Wattrisse, A. Chrysochoos, J.M. Muracciole, M. Nemoz-Gaillard, J. Caillard, Analysis of strain localization during tensile tests by digital image correlation, Experimental Mechanics 41 (2001) 29–39.
[17] A. Chrysochoos, V. Huon, F. Jourdan, J.M. Muracciole, R. Peyroux, B. Wattrisse, Use of full-field digital image correlation and infrared thermography measurements for the thermomechanical analysis of material behaviour, Strain 46 (2001) 117–130.
[18] A. Chrysochoos, H. Louche, An infrared image processing to analyse the calorific effects accompanying strain localization, International Journal of Engineering Science 38 (2000) 1759–1788.
[19] A. Chrysochoos, B. Wattrisse, J.M. Muracciole, Y. El Kaim, Fields of stored energy associated with localized necking of steel, Journal of Mechanics of Materials and Structures 4 (2009) 245–262.
[20] A. Benaarbia, A. Chrysochoos, G. Robert, Influence of relative humidity and loading frequency on the PA6.6 cyclic thermomechanical behavior: part I. Mechanical and thermal aspects, Polymer Testing 40 (2014) 290–298.
[21] B. Halphen, Q.S. Nguyen, On the generalized standards materials (in French), Journal de Mécanique 14 (1975) 39–63.
[22] V. Honorat, S. Moreau, J.M. Muracciole, B. Wattrisse, A. Chrysochoos, Calorimetric analysis of polymer behaviour using a pixel calibration of an IRFPA camera, Qirt Journal 2 (2005) 153–171.
[23] N. Ranc, A. Blanche, D. Ryckelynck, A. Chrysochoos, POD preprocessing of IR thermal data to assess heat source distributions, Journal of Experimental Mechanics (2014) 1–15. Springer US.